Investigation of erbium dopant distribution in silica optical fibers with fluorescence-based measurements using a near-field scanning microscope

Optical Engineering

OpticalEngineering.SPIEDigitalLibrary.org

Investigation of erbium dopant distribution in silica optical fibers with fluorescence-based measurements using a near-field scanning microscope

Fotios Sidiroglou
Ann Roberts
Greg W. Baxter

SPIE.

Investigation of erbium dopant distribution in silica optical fibers with fluorescence-based measurements using a near-field scanning microscope

Fotios Sidiroglou,[a] Ann Roberts,[b] and Greg W. Baxter[a,*]
[a]Victoria University, College of Engineering and Science, Optical Technology Research Laboratory, Telecommunications Electronics Photonics and Sensors, PO Box 14428, Melbourne, Victoria 8001, Australia
[b]University of Melbourne, School of Physics, Melbourne, Victoria 3010, Australia

Abstract. High spatial resolution information of the rare-earth dopant distribution in optical fibers enriches our understanding of the fiber manufacture processes and enables improvement in the design of active photonic devices including optical fiber lasers and amplifiers. Here, data from an investigation of the backscattered fluorescence signal off the end-face of an erbium (Er^{3+}) doped silica optical fiber obtained with a near-field scanning optical microscope (NSOM) are presented. It has been recently confirmed via a theoretical model that information about the relative Er^{3+} ion distribution in fibers can be inferred by simply monitoring the fluorescence signal originating from the de-excitation of specific energy levels in the investigated samples. A comparison of the Er^{3+} ion distribution profiles extracted from the fluorescence measurements acquired through the NSOM system with those obtained from the application of a powerful analytical ion probe is also presented. [DOI: 10.1117/1.OE.53.12.126104]

Keywords: optical fiber; rare-earth; imaging; distribution.

Paper 141421 received Sep. 14, 2014; accepted for publication Nov. 18, 2014; published online Dec. 5, 2014.

1 Introduction

The ongoing evolution of active photonic devices—fiber lasers, fiber amplifiers and sensors—has a strong and growing influence on our daily lives which often goes unrecognized. Such devices are now readily used across numerous fields including, telecommunications, industrial materials processing, medicine, environmental and medical monitoring, the oil and gas industries, and many others. Recent global trends demand superior performance of active photonic devices; this demand will continue to rapidly grow along with the potential for additional industrial applications over the next few years. Since the development of the erbium doped fiber amplifier (EDFA)[1] for the communications industry, active optical fiber technology has been dominated by alumino-germanate enriched silica glass as the host material into which is incorporated rare-earths (REs) as active ions. Fiber fabrication is similarly monopolized by the originally conceived fabrication processes, where in the most traditional scheme, RE doped silica optical fibers are manufactured via the application of the modified chemical vapor deposition (MCVD)[2] and solution doping techniques.[3]

Likewise, information from the postfabrication characterization processes is normally based on imaging techniques borrowed from the areas of analytical chemistry and materials science. In the most traditional approach to date, the concentration of dopants and their distribution, together with the refractive index profile (RIP) and other parameters, are measured in the fiber preform prior to the fiber drawing process.[4–8] The resultant dopant concentration and distribution are then scaled down to match the drawn fiber dimensions assuming that no defects or redistribution during the drawing process influence the resulting fiber profile. However, this procedure overlooks such effects as elemental diffusion that takes place because of the high temperature environment created during the drawing process, which can alter the final glass matrix including the RIP.[9] As a result, it is not always valid to simply relate the dopant concentration profile extracted from preform measurements to fiber dimensions. A technique that will directly extract the information from the drawn fiber is clearly the only way to guarantee the accuracy of data.

Therefore, new approaches have emerged to directly provide high spatial resolution information of the RE dopant distribution from the investigation of optical fibers. Once again, in most of these studies, the imaging systems used were borrowed from analytical chemistry and materials science.[9–13] Although these techniques offer adequate spatial imaging resolution for the direct investigation of optical fibers, and they can even offer information for the distribution of other dopants within the fiber core region, they normally require complex and time-consuming sample preparation and the use of high cost instrumentation.

In the case of some RE-doped optical fibers (i.e., Er^{3+}-doped), such complexities and practical limitations can be overcome by using optical imaging schemes.[14–17] In most cases, the intensity of the backscattered fluorescence originating from the de-excitation of the $^2H_{11/2}$ and $^4S_{3/2}$ upper energy levels (Fig. 1) is monitored and is taken as an indication of the local dopant concentration of the Er^{3+} ions at a point. By scanning the excitation beam across the center of the fiber core, two-dimensional images or line scans of the

*Address all correspondence to: Greg W. Baxter E-mail: gregory.baxter@vu.edu.au

0091-3286/2014/$25.00 © 2014 SPIE

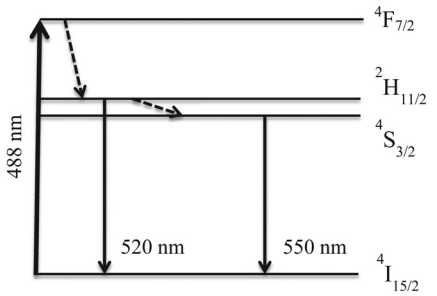

Fig. 1 Partial energy level diagram for Er^{3+} in silica illustrating the levels important to the current study. Solid arrows represent radiative transitions and dashed arrows nonradiative decay.

relative Er^{3+} ion distribution can be acquired. However, care must be taken regarding the reliability of the intensity-based measurements given that cooperative effects are common in RE doped fibers and may yield incorrect values of dopant concentration.[18] Using a simple theoretical study of the spectroscopic characteristics of Er^{3+} doped silica optical fibers, we recently confirmed that information about the Er^{3+} ion distribution in optical fibers can be obtained by exciting the Er^{3+} ions using a 514-nm source and then monitoring the intensity of the backscattered fluorescence signal (540 to 560 nm) originating from the radiative transition of ions between the $^4S_{3/2}$ upper energy level and the ground state. In the work presented here, we extend the relevance of this theoretical model as previously applied to the case where a confocal optical microscope fluorescence intensity confocal optical microscopy (FICOM) was used[16,17] to our current effort to improve spatial resolution using a near-field scanning optical microscope (NSOM).

A previous NSOM study deduced the relative Er^{3+} ion distribution in optical fibers under 488-nm excitation by monitoring the 1550-nm fluorescence signal originating from the de-excitation of ions from the $^4I_{13/2}$ energy level.[19] However, as the ion density increases, the probability for two neighboring ions in the $^4I_{13/2}$ level to interact also increases and the ion density in that level ceases to be linearly proportional to the total ion population of the system. That is, the ion density can no longer be directly inferred from the intensity of the fluorescence signal. In contrast, in this work, the relative Er^{3+} ion distribution in optical fibers is achieved by monitoring the intensity of the backscattered fluorescence originating from the de-excitation of the $^2H_{11/2}$ and $^4S_{3/2}$ (540 to 560 nm) upper energy levels. A linear relationship between ion concentration and the measured fluorescence signal at the 550-nm region has been experimentally and theoretically shown to exist.[17] Therefore, the ion population of the $^4S_{3/2}$ energy state remains linearly dependent on the total ion population even in the presence of possible inter-ionic upconversion events in the lower energy levels. Therefore the resulting fluorescence signal can be relied upon as a direct measure of the relative ion population.

2 Experimental Method

2.1 *Fiber Samples*

Based on the principle of operation of the imaging scheme outlined in our previous work,[16,17] a commercially available NSOM system was employed to investigate the Er^{3+} ion distribution in an experimental EDFA sample acquired from the Laboratoire de Physique de la Martiére Condensée. From

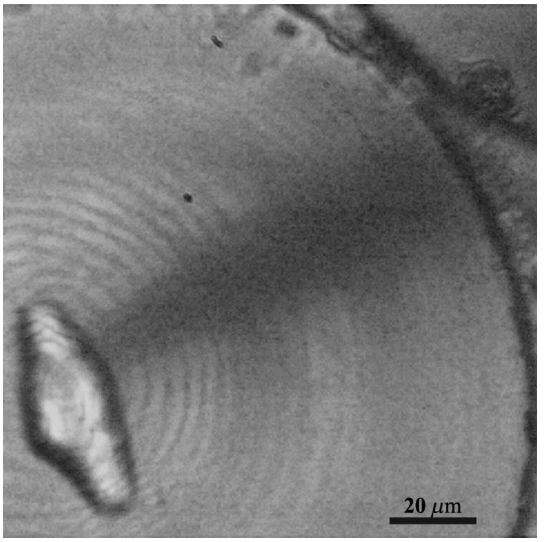

Fig. 2 An optical image of the polished end-face of the erbium doped fiber amplifier (EDFA) fiber sample prior to near-field scanning optical microscope (NSOM) imaging. Also present is the out-of-focus reflection of the NSOM probe tip (dark shade around the center of the picture) and the distinct Newton's rings that are known to manifest themselves under NSOM illumination.

previous studies, it was known that the particular sample contained a distinctive asymmetric configuration, which was thought to be the outcome of an unsuccessful collapse during the fabrication process. The fiber was fabricated using the MCVD technique with the RE ions being incorporated via solution doping. An estimated Er^{3+} concentration of ~7600 ppm was incorporated into the silica core matrix together with a number of network modifiers such as germanium-, aluminum-, and phosphorus oxides. Measurements were performed on the freshly polished end-face of thin fiber slices (Fig. 2), which were prepared using the previously documented polishing technique.[9] The fiber had an outside diameter of roughly 210 μm while the core was approximately 40-μm long by 20-μm wide.

2.2 *Near-Field Scanning Optical Microscope Set-Up*

The end-face of the prepared samples was examined with the help of a modified Nanonics NSOM/SPM-100TM scanning probe configuration (Fig. 3). This system integrates an upright optical microscope (Nikon Eclipse 300 W) for conventional optical imaging, while cantilevered optical fiber NSOM probes were simultaneously incorporated for the near-field and topographic assessment of the samples. NSOM is now an established technique to achieve image resolution beyond the diffraction limit.[20] All probes (Nanonics) were fabricated with the known micropulling technique from an optical fiber manufactured for single-mode operation over the 488 to 514 nm range. The sides of the probe tip were aluminum/chromium coated and a number of different size aperture probes (200, 150, 100, and 50 nm) were employed over the course of the investigation of the samples. The accuracy of the measurement is indicated by the probe diameter while the single-mode operation is important for the successful transport of light to and from the specimen.

During the investigation, the 30-μm thick sliced optical fiber slices were placed on the inbuilt Nanonics 3-D FlatscanTM scanner, so that the sample area was raster

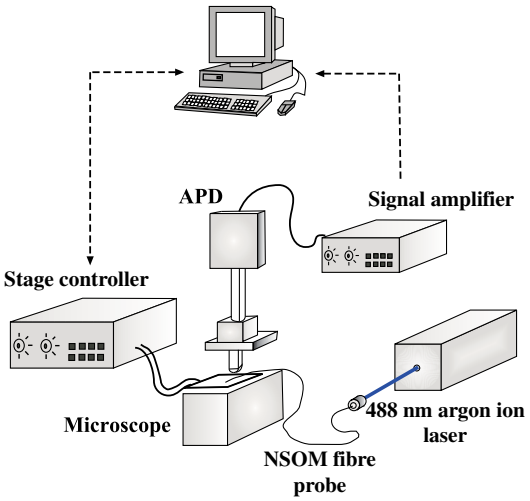

Fig. 3 Schematic diagram of the NSOM experimental arrangement.

scanned under a fixed NSOM probe. The probe-sample distance was regulated by exploiting the normal-force sensing capability of the probe tip by monitoring the reflected 670-nm laser diode signal off the side of the probe. A phase sensitive detector positioned on the opposite side of the NSOM head was used to monitor the 670-nm reflected signal and in the process to regulate the probe-sample separation. Near-field images of the samples were obtained by operating the NSOM system in the reflection mode by scanning the sample under the probe in the noncontact mode. The Er^{3+} ions were excited with direct pumping from a 488 nm wavelength from an air-cooled argon-ion laser (Uniphase, model 2013), which was injected through the coupling optics at the free end of the NSOM fiber probe. During data acquisition, both the reflected signal and induced backscattered fluorescence were collected in the far-field by a 50× long working distance objective (Nikon LPLAN SLWD $50\times/0.45$), which was directly positioned above the NSOM stage. The signal was then spectrally analyzed with the help of appropriate filters before it reached an avalanche photodiode (APD) (Perkin Elmer Optoelectronics, SPCM—AQR—15), mounted at the end of an optical path tube of the microscope. The detected APD signal was amplified using a Nanonics electrical signal amplifier and was finally saved on a remote computer where image formation was achieved.

2.3 *Experimental Challenges*

A strong motivation for this investigation is the potential to obtain superior sub-diffraction limited resolution images by exploiting the small size of the aperture probes used in the NSOM technique. Unfortunately the NSOM arrangement used results in low light levels and introduces stray light contamination. This made the task of generating, isolating and then detecting the desired fluorescence signal, the de-excitation of the $^4S_{3/2}$ level, quite challenging.

The 488-nm excitation source and the 670-nm laser line used in the process of monitoring the location of the probe tip relative to the sample were immediately identified as the two main sources that could interfere with the measured fluorescence signal. Using an optical spectrum analyzer (ANDO, AQ—6310B) (OSA), both light sources were first spectrally evaluated. A series of spectra were obtained by coupling light from either source into an optical fiber and then analyzing it with the OSA. These scans were repeated after placing various filter arrangements before the coupling optics in order to test the influence of each filter on the measured emission of each source. From the retrieved spectra, it was found that both light sources exhibited spectral characteristics that would require more than one optical filter for the adequate elimination of those lines. This was able to be achieved without interfering with the acquisition of the 550-nm peak.

Specifically, in the case of the 488-nm excitation source, other known argon-ion lines were emitted by the laser. Although the incorporation of a super notch optical filter (Kaiser Optical Systems, H SPF—488.0–1.0) efficiently blocked the primary 488-nm argon-ion line and partly diminished the strength of the other wavelengths, it was still possible that some light could propagate through the probe to the sample area and then to the APD. However, by adding a 550-nm interference bandpass filter (Olympus IF) in the optical path between the 488-nm notch filter and the APD, efficient blocking of all secondary lines was achieved.

Blocking the laser diode (located on the NSOM head) with the 670-nm central wavelength proved to be a greater challenge. As part of the process of monitoring the location of the NSOM probe, light from a 670-nm laser diode is focused on the curvature point of the probe, while the scattered light is collected by a photo-sensitive diode. However, light is scattered in all directions around the probe including the sample area where data acquisition takes place. This unconfined source of light has a relatively high intensity as well as having a relatively large bandwidth. A 550-nm bandpass optical filter with a high attenuation (with an optical density greater than 5) in the region outside the 550-nm range was required to efficiently block the interfering laser diode signal. Alternatively, a high attenuation blocking filter with a large bandwidth could be employed to prevent the 670-nm light from interfering with the detection of the fluorescence peak. However, no filters exhibiting such characteristics were commercially available.

In order to address this issue, a 670-nm (20-nm FWHM) line filter (Newport, 05LF20—670) was first immediately placed in front of the output of the laser diode so that the emission band was confined to a narrow range of wavelengths around the central emission. Although the placement of this filter appeared to substantially reduce the intensity of the 670-nm line, the remaining signal was of sufficient strength to maintain proper function of the probe monitoring process. During data acquisition, a 676-nm notch filter (Iridian, ZX000287-001-03-01 676) was also positioned between the collecting optics and the APD, which significantly reduced any reflected signal from the NSOM probe reaching the APD.

2.4 *Data Acquisition*

Using the 50× "super long distance" microscope objective, the sample area was located, while the flatness and surface quality of the sample were examined prior to the investigation of the sample. A 200-nm diameter aperture cantilevered fiber probe (Nanonics CFN—200) was then placed on the NSOM stage and initially kept at a relatively long distance away from the sample. Light from the argon-ion laser

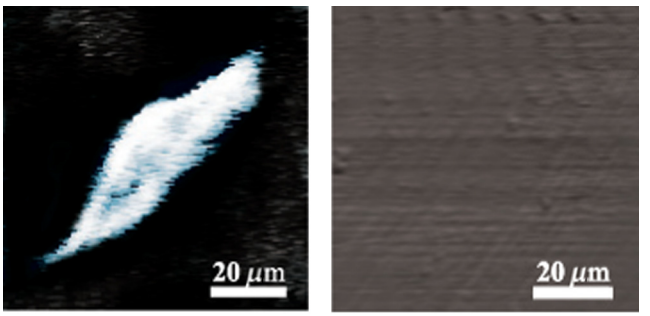

Fig. 4 Cross-sectional images of the polished end-face of the investigated fiber samples with the NSOM system. (a) The NSOM image, (b) the topographical image.

($\lambda = 488$ nm, $P \sim 10$ mW) was coupled into the 200-nm aperture NSOM probe. The far-field optics were focused at the end of the probe tip and using the light coming out of the probe the APD was aligned. Some readjustments regarding the resonant frequency were then made before the probe tip was brought in close proximity to the sample so that scanning could commence.

The sample was then raster scanned underneath the NSOM probe over an area that covered the core region of the fiber sample. In the area where the Er^{3+} ions are located, the incident pump excites the ions from the ground state to upper energy levels. Backscattered fluorescence centered on 550 nm resulting from the de-excitation of the $^4S_{3/2}$ energy level was spectrally differentiated with the use of the aforementioned filter arrangements and detected with the APD. The intensity of the backscattered fluorescence from each point was taken as an indication of the local dopant concentration.

The 550-nm backscattered fluorescence is expected to be proportional to the erbium ion concentration since the process of excitation of the $^4F_{7/2}$ level and the subsequent de-excitation of the $^4S_{3/2}$ level is free from possible excited state absorption, cross-relaxation or up-conversion effects as previously shown.[17] Fluorescence images displaying the relative erbium ion distribution for a cross section of the examined fibers were realized with subwavelength resolution. In addition, since the operation of the cantilevered NSOM probe is based on the operation of an atomic force microscope, valuable information regarding the topography of the investigated area was simultaneously obtained.

3 Results

Employing the method described above the end-face of the freshly polished fiber slices was thoroughly examined on a number of occasions. Probes with apertures of 200 nm were used in most cases, although scans using smaller size probes were also performed; however, these were less successful due to the lower intensities that they produced. NSOM and topographic information were simultaneously recorded in each case for variable integration times while variable size images were formed.

As a consequence of the weak fluorescence signal, which was further reduced by the many optical filters used as part of the light filtering process, the acquisition of the NSOM signal was not always possible. However, several images were obtained and processed with the Quartz instrumentation software. An example of a successful scan is shown in Fig. 4. This cross-sectional image [Fig. 4(a)] of the experimental EDFA sample shows the core region along with the surrounding cladding having a 512×512 pixel size and covering an area of 80×80 μm with a spatial resolution on the order of the probe aperture size used (~200 nm). Also presented here is an image of the topography of the investigated area [Fig. 4(b)], showing that it is optically flat and free from any artifacts that could disturb the acquisition of the optical signal.

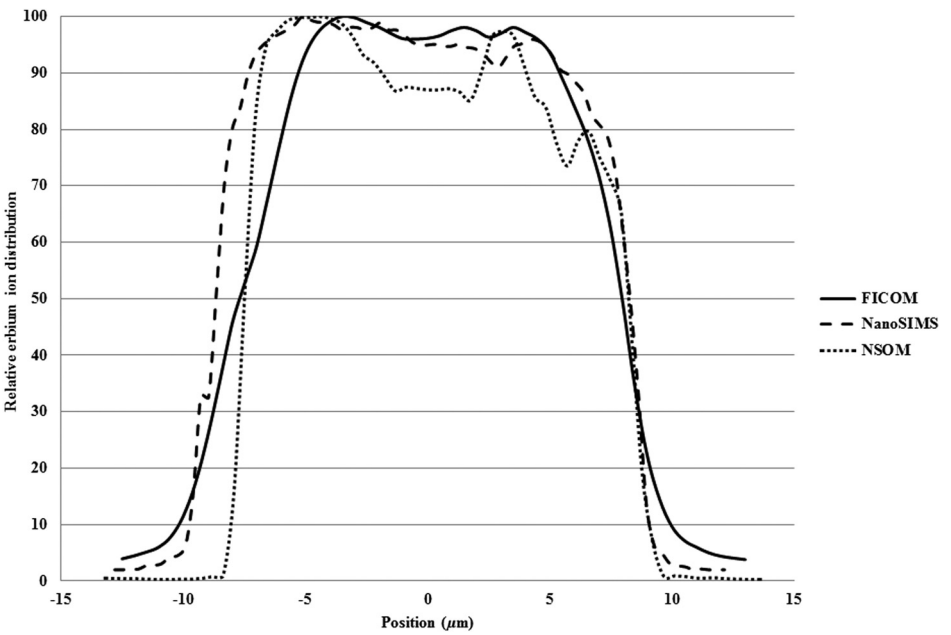

Fig. 5 Normalized transverse profiles through the center of the fiber showing the relative erbium ion distribution in the same EDFA sample, acquired from the application of the microfluorescence (continuous line),[16] nano secondary ion-mass spectrometry (NanoSIMS) (dashed line)[9] and NSOM (dotted line) techniques.

4 Discussion

Information regarding the asymmetric configuration and opto-geometric parameters of this fiber is clearly visible and in good qualitative agreement with data acquired with the previously demonstrated techniques, FICOM, and high resolution secondary ion-mass spectrometry (nanoSIMS)[9,16] (Fig. 5). Furthermore, the increased degree of spatial resolution that is made available using the NSOM technique (~200 nm) reveals superior information on the well-known concentration depletion dip that occurs at the center of the fiber core region.

However, it should be noted that, in some cases, the repeatability of the detected fluorescence signal appeared to be susceptible to the low signal-to-noise ratio and other environmental factors (stray light contamination, excessive usage of optical filter configurations, etc). However, it is expected that a near resonant pumping scheme employing a 514-nm source (rather than 488 nm) could possibly result in a stronger fluorescence signal as a consequence of the higher absorption coefficient that characterizes this absorbing event.

Other difficulties that were encountered during the scanning of other fibers resulted from the flatness and cleanliness of the investigated area of the thin polished mount. Figure 6 represents such a case, where the scanning process has been affected by the existence of a dust cluster located on the end-face of the examined core region. Due to the presence of the particle, the probe moves over the particle and away from the end-face of the fiber, which translates to the absence of optical information at that point (upper image of Fig. 6) and the formation of a signal peak in the topographical image (lower image of Fig. 6). Such issues can be successfully avoided by ensuring that topographical scans are included in the experimental procedure.

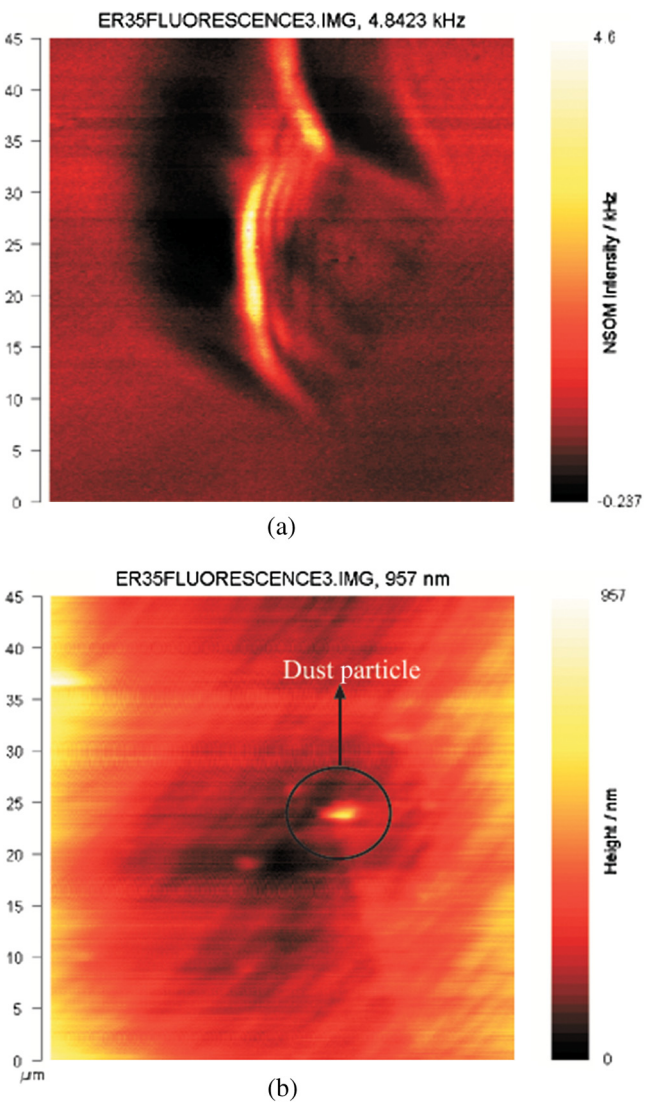

Fig. 6 NSOM and topography images illustrating the existence of a dust particle on the end-face of the investigated area. (a) NSOM image, (b) topography image.

5 Conclusion

The Er^{3+} ion distribution within an experimental EDFA optical fiber sample has been measured using a modified commercially available NSOM configuration. Dopant-ion information with superior spatial resolution (on the order of the probe aperture size used) was achieved with this technique. Several NSOM and topographical images were successfully acquired, showing the relative Er^{3+} ion distribution in the core of the investigated samples. The generated distribution profile is in good qualitative agreement with information obtained using other imaging schemes, but with a substantially improved spatial resolution. Although the application of this technique has only been demonstrated for the investigation of the Er^{3+} ion distribution in optical fibers, it is expected that other REs may be examined in a similar manner provided that certain spectroscopic characteristics can be directly linked with the distribution of the investigated RE ions.

Many practical difficulties that could potentially increase the ambiguity and affect the consistency in obtaining this type of data were identified and overcome in this work, highlighting the fact that care must be taken in using this technique.

There is a significant merit in seeking to further develop this technique, particularly in improving the achieved resolution to 50 nm or less. With such a resolution, important information on the nanostructure of RE optical fibers will be within reach.

References

1. R. J. Mears et al., "Low-noise erbium-doped fibre amplifier operating at 1.54 μm," *Electron. Lett.* **23**(19), 1026–1028 (1987).
2. J. MacChesney et al., "Preparation of low loss optical fibers using simultaneous vapor phase deposition and fusion," in *Proc. 10th Int. Congress on Glass*, Vol. 6, pp. 40–45, Ceram Society of Japan, Tokyo (1974).
3. J. E. Townsend, S. B. Poole, and D. N. Payne, "Solution-doping technique for fabrication of rare-earth-doped optical fibres," *Electron. Lett.* **23**(7), 329–331 (1987).
4. N. Kagi, A. Oyobe, and K. Nakamura, "Gain characteristics of Er^{3+} doped fiber with a quasi-confined structure," *J. Lightwave Technol.* **8**(9), 1319–1322 (1990).
5. M. Shimizu et al., "Concentration effect on optical amplification characteristics of Er-doped silica single-mode fibers," *IEEE Photon. Technol. Lett.* **2**(1), 43–45 (1990).
6. W. L. Barnes et al., "Absorption and emission cross section of Er^{3+} doped silica fibers," *IEEE J. Quantum Electron.* **27**(4), 1004–1010 (1991).
7. T. Kashiwada et al., "Erbium-doped fiber amplifier pumped at 1.48 μm with extremely high efficiency," *IEEE Photon. Technol. Lett.* **3**(8), 721–723 (1991).

8. B. J. Ainslie et al., "The fabrication, assessment and optical properties of high-concentration Nd^{3+}- and Er^{3+}-doped silica-based fibres," *Mater. Lett.* **6**(5–6), 139–144 (1988).
9. F. Sidiroglou et al., "Simultaneous multidopant investigation of rare-earth-doped optical fibers by an ion microprobe," *Opt. Lett.* **31**(22), 3258–3260 (2006).
10. M. Hellsing et al., "ToF-SIMS imaging of dopant diffusion in optical fibers," *Appl. Surf. Sci.* **203–204**, 648–651 (2003).
11. A. C. Pugh, R. P. Stratton, and D. B. Lewis, "Investigation of elemental diffusion during the drawing and heat treatment of glass optical fibers," *J. Mater. Sci.* **29**(4), 1036–1040 (1994).
12. S. Rogard et al., "Non-destructive concentration measurements of erbium-doped zblan fluorozirconate glass," *Opt. Mater.* **4**(5), 557–563 (1995).
13. R. Citron and J. Kropf, "X-ray absorption spectroscopy of Yb-doped optical fibers," Journal of Undergraduate Research, U.S. Department of Energy, 8, 39–47, http://martha7mo.files.wordpress.com/2013/04/jur_2008.pdf (2008).
14. B. P. Petreski et al., "Imaging concentration profiles of praseodymium-doped optical fibres," *Electron. Lett.* **33**(10), 889–891 (1997).
15. A. Othonos, J. Wheeldon, and M. Hubert, "Determining erbium distribution in optical fibers using phase-sensitive confocal microscopy," *Opt. Eng.* **34**(12), 3451–3455 (1995).
16. F. Sidiroglou et al., "Microcharacterisation of erbium-doped fibers using a Raman confocal microscope," *Opt. Express* **13**(14), 5506–5512 (2005).
17. F. Sidiroglou, A. Roberts, and G. W. Baxter, "Probing the erbium ion distribution in silica optical fibers with fluorescence based measurements," *J. Non-Cryst. Solids* **357**(22–23), 3847–3852 (2011).
18. I. R. Perry, A. C. Tropper, and J. R. M. Barr, "Micro-fluorescence profiling of erbium-doped fibre preforms," *J. Lumin.* **59**(1–2), 39–49 (1994).
19. J. K. Trautman et al., "Image contrast in near-field optics," *J. Appl. Phys.* **71**(10):4659–4663 (1992).
20. U. C. Fischer, U. T. Dürig, and D. W. Pohl, "Near-field optical scanning microscopy in reflection," *Appl. Phys. Lett.* **52**, 249 (1988).

Fotios Sidiroglou received his PhD degree in physics from the University of Melbourne, Australia, in 2007. He joined the OTRL at Victoria University in 2009 and since then has contributed to fiber optics by developing/utilizing imaging set-ups for the investigation of RE-ion distributions in fibers. He is now looking into feeding back the findings from these studies in advancing the existing fiber fabrication techniques. His research interests include the development of optical-based sensors.

Ann Roberts received her BSc and PhD degrees in physics from the University of Sydney. After a postdoctoral position at Cornell University, she took up an academic position in the School of Physics at the University of Melbourne. She has diverse research interests in physical optics and photonics, including imaging, nanophotonics, and plasmonics. She is a fellow of the Australian Institute of Physics, senior member of the OSA, and past-president of the Australian Optical Society.

Greg W. Baxter received his BSc and PhD degrees in physics from the University of Melbourne and currently is a research professor with Victoria University. He has considerable experience with the fabrication, characterization, and application of optical fiber technology. His research interests include the development of optical fibers as sensors, the submicron characterization of optical fiber devices such as fiber Bragg gratings and the fabrication of rare-earth doped optical fiber.